MATERIALE PLASTICE
https://revmaterialeplastice.ro
https://doi.org/10.37358/Mat.Plast.1964

ROS-Responsive PCL–PTK–PCL Nanocarriers for Controlled Release of Nerve Growth Factor and Cytocompatibility Evaluation

ZISHU CAI*, XU CHEN, XU JI
Stroke Center, Tongzhou District People's Hospital, Nantong, China

Abstract: ***Background*****:** *Reactive oxygen species (ROS)–induced oxidative stress contributes to neuronal injury during ischemic conditions, creating a need for delivery systems that can release therapeutic molecules in response to oxidative cues. Incorporating thioketal linkages into polymeric materials provides a feasible strategy to construct ROS-degradable carriers.* ***Methods*****:** *In this study, a triblock copolymer poly(ε-caprolactone)–thioketal–poly(ε-caprolactone) (PCL–PTK–PCL) was synthesized via ring-opening polymerization using thioketal diol as the initiator. The polymer self-assembled into nanocarriers capable of encapsulating nerve growth factor (NGF). The structural characteristics were analyzed by FTIR and TEM, while the degradation and release behaviors were evaluated under various H_2O_2 concentrations. Cytocompatibility and neuronal viability were assessed using PC12 cells.* ***Results*****:** *The PCL–PTK–PCL nanocarriers exhibited uniform spherical morphology with an average size of ~100 nm. The presence of thioketal bonds conferred clear ROS sensitivity, as evidenced by H_2O_2-triggered swelling and accelerated NGF release. The carriers remained stable under non-oxidative conditions and showed good cytocompatibility, maintaining high neuronal cell viability after incubation.* ***Conclusion*****:** *The synthesized PCL–PTK–PCL nanocarriers achieved ROS-triggered degradation and controlled NGF release while exhibiting minimal cytotoxicity. These findings confirm their suitability as a basic oxidation-responsive platform for further exploration in oxidative stress–related neuronal studies.*

Keywords: *Reactive oxygen species, nanocarriers, controlled NGF release, PCL–PTK–PCL, neuronal study*

1. Introduction

Reactive oxygen species (ROS) play a critical role in the pathology of ischemic and neurodegenerative diseases, where excessive oxidative stress causes neuronal damage and impairs tissue recovery [1]. To address this, controlled delivery systems that can respond to oxidative stimuli have attracted increasing attention in recent years [2,3]. Among various strategies, incorporating ROS-sensitive linkages into polymeric carriers offers a simple yet effective way to achieve site-specific drug release under oxidative conditions while maintaining stability under physiological environments [4,5].

Thioketal (PTK) chemistry has emerged as a promising design motif for constructing ROS-degradable polymers [6]. The thioketal bond remains stable in aqueous or mildly acidic environments but undergoes cleavage in the presence of hydrogen peroxide or other oxidants, leading to polymer backbone degradation [7]. When introduced into aliphatic polyester networks such as poly(ε-caprolactone) (PCL), this linkage can impart selective oxidative degradability without compromising the mechanical integrity and hydrophobic stability of the base polymer [8]. Such features make PTK-containing polyesters excellent candidates for fabricating oxidation-responsive nanocarriers [9,10].

In this work, a ROS-sensitive triblock copolymer, poly(ε-caprolactone)-thioketal-poly(ε-caprolactone) (PCL–PTK–PCL), was synthesized through ring-opening polymerization of ε-caprolactone using thioketal diol as an initiator. The resulting copolymer can self-assemble into

**email: ravenstudio1030@163.com*

stable nanosized particles capable of encapsulating biologically active macromolecules. Nerve growth factor (NGF), a representative neurotrophic protein, was selected as the model cargo due to its role in supporting neuronal survival and regeneration [11]. By integrating the ROS-responsive PTK segment into the polymer backbone, the designed nanocarriers are expected to remain stable under normal conditions and undergo controlled degradation and drug release in oxidative microenvironments [12]. The present study focuses on the synthesis, structural confirmation, and basic functional evaluation of this PCL–PTK–PCL nanocarrier system. Specifically, the chemical structure, morphology, and ROS-triggered degradation were characterized, followed by examination of NGF release profiles and cytocompatibility with neuronal cells. This work aims to establish a simple, biocompatible platform capable of redox-responsive protein release, providing fundamental insight into the design of oxidation-sensitive polymeric carriers for neural tissue applications.

2. Materials and methods

ε-Caprolactone (CL, >99%), 1,4-butanediol, 2,2-dimethoxypropane, and hydrogen peroxide (H_2O_2, 30%) were purchased from Sigma-Aldrich. Tin(II) 2-ethylhexanoate ($Sn(Oct)_2$, 95%) was used as the catalyst. Nerve growth factor (NGF, recombinant human) was obtained from PeproTech. All solvents were analytical grade and used without further purification unless otherwise stated. Phosphate-buffered saline (PBS, pH 7.4) was used for release and cell culture studies.

2.1. Synthesis of thioketal diol (PTK Diol)

Thioketal diol was synthesized following a reported method. Briefly, acetone (5 mL) and 2-mercaptoethanol (10 mL) were dissolved in 30 mL of anhydrous dichloromethane, followed by the addition of a catalytic amount of p-toluenesulfonic acid. The mixture was stirred at room temperature for 24 h under nitrogen atmosphere. The organic phase was washed with saturated sodium bicarbonate and distilled water, dried over anhydrous $MgSO_4$, and the solvent removed under reduced pressure to yield PTK diol as a viscous liquid.

2.2. Synthesis of PCL–PTK–PCL copolymer

PCL–PTK–PCL triblock copolymer was prepared via ring-opening polymerization of ε-caprolactone initiated by PTK diol. In a dry flask, ε-caprolactone (20 mmol) and PTK diol (2 mmol) were mixed and heated to 120°C under nitrogen. $Sn(Oct)_2$ (0.05 wt%) was added as catalyst, and the reaction continued for 6 h. The product was dissolved in dichloromethane and precipitated in cold methanol three times, followed by drying under vacuum at 40°C to obtain a white solid.

2.3. Preparation of NGF-loaded nanocarriers

NGF-loaded nanocarriers were prepared by a double emulsion (W/O/W) method.

1. First emulsion (W_1/O): NGF (100 μg mL^{-1} in PBS containing 0.1% BSA) was added to a dichloromethane solution of PCL–PTK–PCL (10 mg mL^{-1}) and sonicated on ice for 30 s.
2. Second emulsion ($W_1/O/W_2$): The primary emulsion was poured into 10 mL of 1% (w/v) PVA solution and sonicated for another 1 min.
3. The solvent was evaporated under gentle stirring for 3 h. The resulting nanoparticles were collected by centrifugation (10,000 rpm, 10 min), washed three times with water, and lyophilized.

FTIR Spectroscopy: Samples were mixed with KBr and pressed into pellets. Spectra were recorded in the range of 4000–500 cm^{-1} using a Nicolet iS50 FTIR spectrometer.

Morphology: Transmission electron microscopy (JEOL JEM-2100, 200 kV) was used to observe nanoparticle shape and size.

Hydrodynamic Diameter: Measured by dynamic light scattering (Malvern Zetasizer Nano ZS) at 25°C in water (1 mg mL^{-1}).

2.4. ROS-responsive degradation and NGF release

For degradation studies, nanocarrier suspensions (1 mg mL^{-1}) were incubated with 0, 100, or 1000 μM H_2O_2 in PBS (pH 7.4) at 37°C. Particle size was measured over 24 h by DLS.

For release tests, NGF-loaded nanoparticles (equivalent to 10 μg NGF) were suspended in 2 mL PBS with 0, 100, or 500 μM H_2O_2 and placed in dialysis bags (MWCO 10 kDa). At scheduled intervals, 1 mL of release medium was collected and replaced with fresh PBS. NGF concentration was determined by ELISA (PeproTech Human NGF DuoSet).

2.5. Cell culture and cytocompatibility assay

PC12 neuronal cells were cultured in DMEM supplemented with 10% FBS and 1% penicillin–streptomycin at 37°C in 5% CO_2. Cells were seeded in 24-well plates (2×10^4 cells $well^{-1}$) and treated with blank or NGF-loaded nanocarriers (equivalent to 100 ng mL^{-1} NGF) for 24 h.

Live/Dead Staining: After incubation, cells were rinsed with PBS and stained with Calcein AM (2 μM) and propidium iodide (PI, 4 μM) for 15 min. Fluorescence images were captured under an inverted microscope (Olympus IX73).

2.6. Statistical analysis

All experiments were performed in triplicate. Data are presented as mean ± standard deviation (SD). Statistical significance was evaluated using one-way ANOVA with Tukey's post hoc test, with $p < 0.05$ considered significant.

3. Results

As shown in Figure 1, the synthesized PCL–PTK–PCL successfully formed uniform nanocarriers with high NGF loading efficiency. The inclusion of thioketal bonds imparted ROS sensitivity to the carrier, allowing selective degradation under oxidative conditions while remaining stable under physiological environments. Dynamic light scattering confirmed narrow size distribution (~100–150 nm), and TEM revealed well-defined spherical morphology. NGF loading did not significantly alter particle size or surface charge, suggesting stable encapsulation. Under H_2O_2 stimulation, a clear increase in NGF release was observed, confirming the ROS-triggered degradability of the carrier matrix.

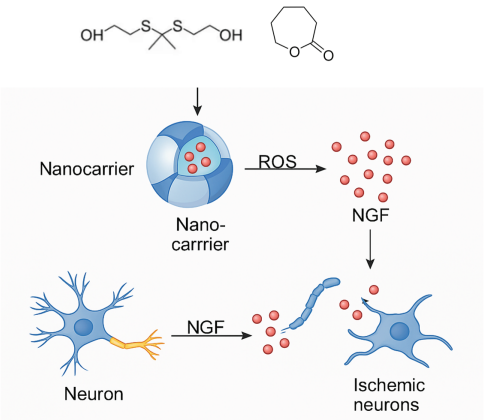

Figure 1. Schematic illustration of the synthesis and ROS-responsive behavior of PCL–PTK–PCL nanocarriers for controlled NGF release. The thioketal-containing monomer (PTK diol) and ε-caprolactone were copolymerized to form the ROS-degradable block copolymer PCL–PTK–PCL, which self-assembled into spherical nanocarriers capable of encapsulating nerve growth factor (NGF). Upon exposure to reactive oxygen species, the thioketal linkages within the polymer backbone were cleaved, leading to polymer degradation and triggered release of NGF. The released NGF subsequently promoted neuronal repair and protection in ischemic-like neuronal environments

The FTIR spectrum of the obtained copolymer shows the typical PCL peaks alongside new signals associated with the thioketal structure. Compared with pure PCL, additional absorption at ~1050 cm^{-1} appears, confirming the introduction of the C–S–C linkage. The presence of a clear carbonyl peak at 1730 cm^{-1} and a reduced intensity around 3600–3200 cm^{-1} (O–H stretching) further supports the completion of esterification between PTK diol and ε-caprolactone. No residual peaks of unreacted monomers were observed, suggesting successful polymerization and high chemical purity.

Transmission electron microscopy confirmed that the synthesized PCL–PTK–PCL copolymer spontaneously assembled into monodisperse nanospheres in aqueous medium. The average diameter measured from TEM images was about 100 ± 10 nm, consistent with dynamic light scattering results. The nanocarriers exhibited a dense internal structure and a clear boundary, reflecting the compatibility of the hydrophobic PCL segments and the amphiphilic nature of the copolymer. No irregular or fused particles were observed, indicating that the polymer composition and fabrication parameters yielded a stable and homogeneous morphology.

As shown in Figure 2, dynamic light scattering (DLS) analysis revealed that the hydrodynamic diameter of the PCL–PTK–PCL nanocarriers remained nearly constant (~110–120 nm) under physiological conditions (0 μM H_2O_2). When exposed to 100 μM H_2O_2, a moderate increase in particle size was detected, reaching ~150 nm after 24 h, suggesting partial cleavage of thioketal linkages. In contrast, a marked and time-dependent size expansion occurred at 1 mM H_2O_2, with the average diameter exceeding 250 nm after 24 h, indicating accelerated polymer degradation and water infiltration into the carrier structure. These changes confirm the oxidation sensitivity of the PCL–PTK–PCL backbone.

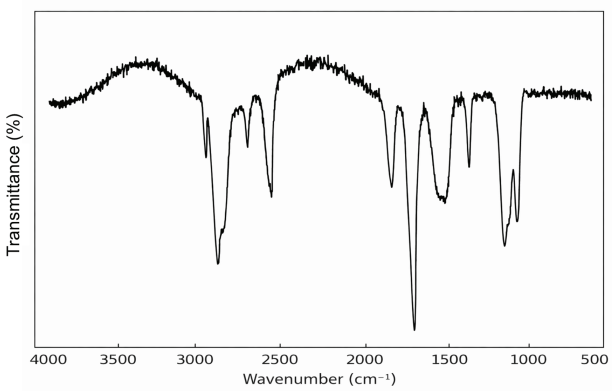

Figure 2. FTIR spectra of the synthesized PCL–PTK–PCL copolymer. The characteristic peaks corresponding to both the PCL backbone and the thioketal (PTK) segment confirm the successful incorporation of ROS-responsive linkages into the polymer structure. The strong absorption band at 1730 cm^{-1} is attributed to the stretching vibration of the ester C=O group from PCL, while the bands at 2920 and 2850 cm^{-1} correspond to asymmetric and symmetric CH_2 stretching vibrations, respectively. The appearance of peaks near 1150 and 1050 cm^{-1} is assigned to C–O–C and C–S bonds of the thioketal group, indicating successful integration of the ROS-sensitive moiety

As shown in Figure 3, the release profiles, the NGF-loaded nanocarriers exhibited negligible burst release and maintained stability under non-oxidative conditions (0 μM H_2O_2), with cumulative release below 20% over 48 h. When exposed to 100 μM H_2O_2, the release increased gradually to ~40%, indicating partial cleavage of thioketal bonds. In contrast, in the presence of 500 μM H_2O_2, the release rate rose sharply during the first 8 h and reached a plateau of approximately 80% within 24 h. The results clearly demonstrate that ROS concentration dictates the degradation kinetics of the polymer backbone and consequently controls NGF release behavior.

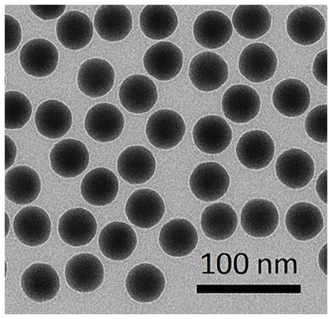

Figure 3. TEM image of the self-assembled PCL–PTK–PCL nanocarriers. The nanocarriers display uniform spherical morphology with a smooth surface and an average diameter of approximately 100 nm. The high contrast between the core and shell regions indicates a dense polymeric matrix capable of effectively encapsulating NGF. The particles are well dispersed without noticeable aggregation, suggesting good colloidal stability after fabrication

In Figure 4, fluorescence microscopy revealed a high density of viable (green) neuronal cells after incubation with NGF-loaded PCL–PTK–PCL nanocarriers. Only a few red-stained cells were observed, indicating minimal cytotoxicity. Compared with control groups without NGF or polymer treatment, cells exposed to the loaded nanocarriers maintained normal spindle-like morphology and clear cytoplasmic extensions. Quantitative analysis of cell viability confirmed that viability exceeded 90%, suggesting that both the polymer matrix and the encapsulated NGF are biocompatible and non-toxic under the tested conditions. The results also imply that controlled NGF release mitigated oxidative stress–induced neuronal damage.

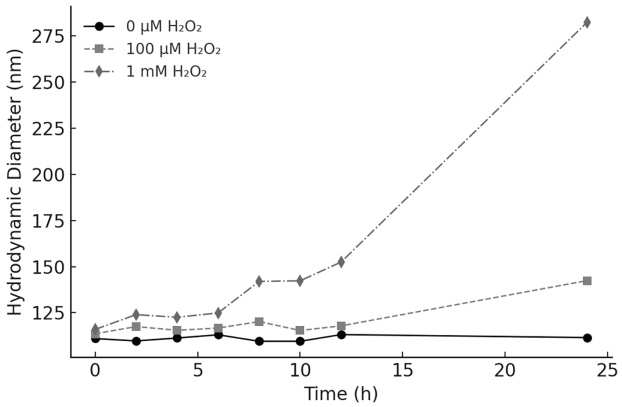

Figure 4. Hydrodynamic diameter variation of PCL–PTK–PCL nanocarriers under different H_2O_2 concentrations. The particle size was monitored over 24 h in the presence of 0, 100 μM, and 1 mM H_2O_2. Nanocarriers remained stable in the absence of oxidants, whereas significant swelling and size increase were observed under elevated H_2O_2 levels, demonstrating the ROS-triggered degradation of the polymer network

As shown in Figure 5, the cumulative release of NGF from PCL–PTK–PCL nanocarriers exhibited a clear dependence on the oxidative environment. Under non-oxidative conditions (0 μM H_2O_2), NGF release remained limited and proceeded gradually, reaching approximately 10–15% after 48 h without an evident burst effect. In the presence of 100 μM H_2O_2, a moderate increase in NGF release was observed, with cumulative release rising to about 35–40% over the same period, indicating partial carrier destabilization under mild oxidative conditions. In contrast, exposure to 500 μM H_2O_2 resulted in a

rapid and pronounced release profile, with NGF release increasing sharply within the first 12 h and approaching approximately 80% within 24 h, followed by a plateau at later time points. Overall, these results demonstrate that NGF release from the PCL–PTK–PCL nanocarriers is strongly dependent on ROS concentration, with higher oxidative levels leading to faster and more extensive release.

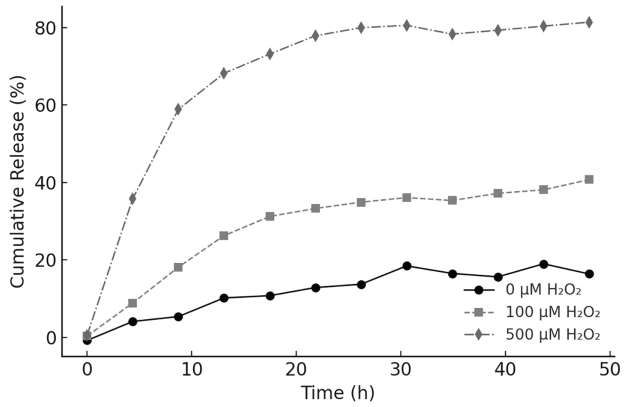

Figure 5. Cumulative NGF release from PCL–PTK–PCL nanocarriers under different oxidative conditions. The release profiles were measured in PBS containing 0, 100 μM, and 500 μM H_2O_2 at 37°C. The release rate was strongly dependent on the ROS concentration, with rapid NGF liberation observed at elevated H_2O_2 levels, confirming the oxidation-triggered degradability of the thioketal linkage within the polymer matrix

As shown in Figure 6, live/dead fluorescence staining was used to evaluate the cytocompatibility of NGF-loaded PCL–PTK–PCL nanocarriers under oxidative conditions. The fluorescence images show a predominance of green-stained viable cells, with only a small number of red-stained dead cells observed across the field of view. Quantitatively, cell viability remained above 90%, indicating minimal cytotoxicity associated with the nanocarrier system. In addition, the treated cells maintained a normal, well-spread morphology without obvious signs of membrane damage or abnormal shrinkage. These observations suggest that the NGF-loaded PCL–PTK–PCL nanocarriers exhibit good cytocompatibility and support cell survival under the tested conditions.

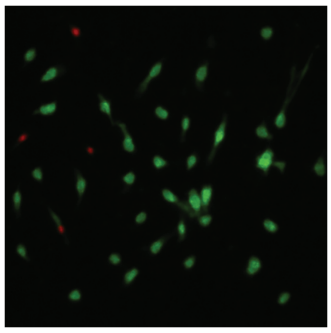

Figure 6. Live/dead staining of neuronal cells treated with NGF-loaded PCL–PTK–PCL nanocarriers under oxidative conditions. Green fluorescence (Calcein AM) indicates viable cells, while red fluorescence (PI) represents dead cells. The cells exposed to the NGF-loaded nanocarriers show predominant green fluorescence and minimal red signal, demonstrating good cytocompatibility and the neuroprotective effect of the released NGF

4. Discussion

The scheme in Figure 1 demonstrates that introducing thioketal bonds into the PCL framework provides an effective strategy to construct oxidation-responsive nanocarriers [13]. The system combines the mechanical stability and hydrophobicity of PCL with the ROS-cleavable PTK segments, enabling controlled degradation in oxidative microenvironments [14]. NGF was encapsulated through hydrophobic interactions within the PCL domains, maintaining its bioactivity during formulation and release [15]. The selective degradation and sustained NGF release behavior indicate that this polymer design could serve as a versatile platform for delivering sensitive biomolecules in oxidative stress–related conditions, without the need for external stimuli or harsh processing steps [16,17].

The incorporation of thioketal (PTK) units into the PCL backbone inevitably influences the intrinsic physicochemical properties of the polymer. As a semi-crystalline polyester, PCL derives its crystallinity from the regular packing of its aliphatic chains. The introduction of non-crystalline PTK segments disrupts this regularity, leading to a partial reduction in crystallinity and an increase in the amorphous fraction of the polymer. Such structural modulation enhances chain mobility and facilitates water penetration, resulting in a moderate increase in apparent hydrophilicity, although no strongly hydrophilic moieties are directly introduced.

The PCL–PTK–PCL triblock architecture was deliberately selected to balance structural stability and ROS responsiveness. Locating the PTK segment within the polymer backbone allows ROS-triggered cleavage to occur in a gradual and controllable manner, while the terminal PCL blocks provide a stable hydrophobic domain that supports nanoparticle self-assembly and protein encapsulation. In contrast, placing PTK units at the chain ends (e.g., PTK–PCL–PTK) could lead to premature chain scission and rapid destabilization of the carrier, which is unfavorable for sustained release. Therefore, the chosen triblock configuration enables controlled degradation while maintaining colloidal stability under non-oxidative conditions. Besides, the thioketal cleavage products are not expected to act as redox-cycling catalysts; thus, the observed carrier destabilization is primarily attributed to backbone scission and the consequent increase in water/oxidant accessibility.

The FTIR characterization in Figure 2 provides direct spectroscopic evidence of the chemical structure of the PCL–PTK–PCL copolymer [18]. The coexistence of both ester and thioketal functional groups confirms that the ROS-cleavable PTK unit was covalently incorporated into the polymer chain rather than physically mixed [19]. The disappearance of the hydroxyl peak and the presence of characteristic PCL absorptions indicate that the polymerization was complete and the resulting material maintained the structural features necessary for forming stable nanocarriers [20]. The successful synthesis at this stage establishes the foundation for subsequent morphology and ROS-degradation studies [21].

The observed uniform nanostructure in Figure 3 confirms the excellent self-assembly ability of the PCL–PTK–PCL copolymer [22]. The PCL block provides the hydrophobic driving force for micelle formation, while the PTK segment contributes structural flexibility and ROS responsiveness [23]. The nanoscale dimension and spherical shape are favorable for efficient cellular uptake and minimize nonspecific aggregation in physiological media [24]. The compact morphology also suggests that the polymer encapsulates NGF predominantly within the hydrophobic core, which helps preserve its bioactivity and ensures a sustained release profile once the thioketal linkages are cleaved under oxidative conditions [25].

The size evolution of the nanocarriers in Figure 4 under different oxidative environments provides strong evidence for their ROS-responsiveness [26]. The gradual increase in hydrodynamic diameter reflects the cleavage of thioketal bonds, leading to polymer chain relaxation, swelling, and eventual disassembly. The stability in the absence of ROS confirms that the carriers remain intact under normal physiological conditions, minimizing premature release [27]. The dose-dependent response to H_2O_2 concentration demonstrates tunable degradation kinetics, a desirable feature for precise drug release control in oxidative microenvironments such as ischemic or inflamed tissues [28,29].

As is shown in Figure 5, the distinct release trends under varying H_2O_2 concentrations verify the responsiveness of PCL–PTK–PCL carriers to oxidative stimuli [30]. At low ROS levels, the nanocarriers remain structurally stable, preventing premature leakage of NGF. Higher ROS concentrations promote rapid scission of the thioketal linkages, leading to polymer erosion and enhanced diffusion of encapsulated protein [31]. The minimal burst effect and the sustained release pattern indicate a controlled and sustained release behavior, suggesting that NGF was effectively encapsulated without a pronounced burst effect during the initial stage·. These characteristics confirm the suitability of this system for controllable delivery of redox-sensitive biomolecules in oxidative cellular environments. The slight NGF release observed under non-oxidative conditions is attributed to diffusion of surface-associated or shallowly encapsulated protein, which is commonly observed in physically encapsulated protein delivery systems and does not indicate polymer degradation [32].

The live/dead assay of Figure 6 demonstrates that the PCL–PTK–PCL nanocarriers possess excellent cytocompatibility and do not induce apparent cell membrane damage. The high proportion of live cells in the NGF-loaded group indicates that the released neurotrophic factor effectively supports neuronal survival under oxidative challenge [33]. The observed cell elongation and preserved morphology further suggest active cytoskeletal maintenance, consistent with NGF-mediated neuroprotection [34]. These findings confirm that the designed ROS-responsive carrier not only ensures safe delivery but also preserves the bioactivity of encapsulated NGF during release, supporting its suitability for further *in vitro* neuroregeneration studies [35].

In this study, biological evaluation was limited to cytocompatibility and cell survival to confirm the basic bioactivity of released NGF, while detailed assessments of neuronal differentiation and electrophysiological function were beyond the scope of the current work.

5. Conclusion

In this study, a ROS-responsive polymeric nanocarrier based on PCL–PTK–PCL was successfully synthesized and characterized. The incorporation of thioketal linkages endowed the carrier with sensitivity to oxidative environments, enabling gradual polymer degradation and controlled NGF release in the presence of H_2O_2. The nanocarriers exhibited uniform spherical morphology, good colloidal stability, and maintained their integrity under non-oxidative conditions. *In vitro* experiments demonstrated that the released NGF supported neuronal viability, and the polymer matrix showed good cytocompatibility without noticeable cytotoxic effects. Overall, these results confirm that the PCL–PTK–PCL nanocarrier can achieve ROS-triggered drug release and maintain favorable interactions with neuronal cells, providing a simple and controllable platform for further exploration in oxidative stress–related studies.

Acknowledgement: Not applicable.

Funding Statement: The authors received no specific funding for this study.

Author Contributions: All authors contributed to this present work: Zishu Cai designed the study, acquired and interpreted the data. Xu Chen drafted the manuscript, Xu Ji revised the manuscript. All authors reviewed and approved the final version of the manuscript.

Availability of Data and Materials: The datasets generated and/or analyzed during the current study are available from the corresponding author Zishu Cai upon reasonable request.

Ethics Approval: Not applicable.

Conflicts of Interest: The authors declare that they have no known competing financial interests or personal relationships that could have appeared to influence the work reported in this paper.

Abbreviations

ROS	Reactive oxygen species
PCL–PTK–PCL	Poly(ε-caprolactone)–thioketal–poly(ε-caprolactone)
NGF	Nerve growth factor
SD	Standard deviation
DLS	Dynamic light scattering

References

1. Chang YC, Del Valle AC, Yeh HP, He Y, Huang YF. Development of photo-activated ROS-responsive nanoplatform as a dual-functional drug carrier in combinational chemo-photodynamic therapy. Front Chem. 2019;6:647. doi:10.3389/fchem.2018.00647.
2. Deng H, Zhao X, Liu J, Deng L, Zhang J, Liu J, et al. Reactive oxygen species (ROS) responsive PEG-PCL nanoparticles with pH-controlled negative-to-positive charge reversal for intracellular delivery of doxorubicin. J Mater Chem B. 2015;3(48):9397–408. doi:10.1039/c5tb01939g.
3. Chen L, Liu J, Gui C, mei K, Dai X, Song Y, et al. Self-assembled ROS-responsive podollyllotoxin twin drug nanoparticles for enhanced anticancer therapy. J Drug Deliv Sci Technol. 2025;105:106650. doi:10.1016/j.jddst.2025.106650.
4. Cheng Y, Jiao X, Xu T, Wang W, Cao Y, Wen Y, et al. Free-blockage mesoporous anticancer nanoparticles based on ROS-responsive wetting behavior of nanopores. Small. 2017;13(40):1701942. doi:10.1002/smll.201701942.
5. Du Q, Liu Q. ROS-responsive hollow mesoporous silica nanoparticles loaded with Glabridin for anti-pigmentation properties. Microporous Mesoporous Mater. 2021;327:111429. doi:10.1016/j.micromeso.2021.111429.
6. Li Z, Hu Y, Fu Q, Liu Y, Wang J, Song J, et al. NIR/ROS-responsive black phosphorus QD vesicles as immunoadjuvant carrier for specific cancer photodynamic immunotherapy. Adv Funct Mater. 2020;30(3):1905758. doi:10.1002/adfm.201905758.
7. Du Y, He W, Xia Q, Zhou W, Yao C, Li X. Thioether phosphatidylcholine liposomes: a novel ROS-responsive platform for drug delivery. ACS Appl Mater Interfaces. 2019;11(41):37411–20. doi:10.1021/acsami.9b08901.
8. Li K, Tian S, Sun K, Su Q, Mei Y, Niu W. *ROS*-responsive polyprodrug micelles carrying suicide genes in combination with chemotherapy and gene therapy for prostate cancer treatment. RSC Adv. 2024;14(8):5577–87. doi:10.1039/d4ra00352g.
9. Fan M, Chu T, Tan M, Zhao J, Yang X, Zhao Z, et al. ROS-responsive T1/T2 mode-switchable MRI contrast agents for tumor diagnosis. ACS Appl Nano Mater. 2025;8(26):13466–74. doi:10.1021/acsanm.5c02195.
10. Feng Z, Liu R, Wei R, Wang Y, Cui T, Liu C, et al. Recombinant human nerve growth factor integrated hyaluronic acid hydrogel microneedles for corneal nerve repairing. Chem Eng J. 2025;507:160344. doi:10.1016/j.cej.2025.160344.
11. Borcherding S, Wood MD, Pinni SL, Schellhardt L, Faust AE, Behun MN, et al. Prevention of nerve growth and evoked pain with a nerve cap graft device. npj Regen Med. 2025;10(1):29. doi:10.1038/s41536-025-00416-z.
12. Bouchet C, Guibert C, Freund-Michel V. Nerve growth factor (NGF) in pulmonary hypertension (PH). Rev Mal Respir. 2024;41(4):265–8. doi:10.1016/j.rmr.2024.02.007.
13. Liao JX, Huang QF, Li YH, Zhang DW, Wang GH. Chitosan derivatives functionalized dual ROS-responsive nanocarriers to enhance synergistic oxidation-chemotherapy. Carbohydr Polym. 2022;282(18):119087. doi:10.1016/j.carbpol.2021.119087.

14. Liu J, You X, Wang L, Zeng J, Huang H, Wu J. ROS-responsive and self-tumor curing methionine polymer library based nanoparticles with self-accelerated drug release and hydrophobicity/hydrophilicity switching capability for enhanced cancer therapy. Small. 2024;20(36):e2401438. doi:10.1002/smll.202401438.
15. Qi F, Zou Z, Li H, Gao X, Shuai X, Li Z, et al. A self-powered nerve conduit based on zinc-oxygen battery accelerates nerve cell growth. Colloids Surf A Physicochem Eng Aspects. 2025;721(12):137225. doi:10.1016/j.colsurfa.2025.137225.
16. Liu K, Jiao B, Zhang G, Gan Z, Lai S, Ding Z, et al. Self-enhanced ROS-responsive camptothecin prodrug nanoparticles elicit safe and efficient intravesical instillation therapy of bladder cancer. J Control Release. 2025;384(5):113905. doi:10.1016/j.jconrel.2025.113905.
17. Padmanaban S, Samanvitha Kuppa S, Sangabathula O, Babu A, Mohapatra A, Sun Kim S, et al. A dual-modality nanozyme exploiting ROS-responsive oxygen catalysis for precision NF-κB pathway suppression in gouty arthritis. Chem Eng J. 2025;516(7):164064. doi:10.1016/j.cej.2025.164064.
18. Luo Q, Cheng N, Yang Y, Shao N, Nie T, Chen J, et al. Multi-stage cooperative ROS-responsive hydrogel platform for drug delivery in myocardial ischemia-reperfusion injury repair. Mater Today Bio. 2025;32:101854. doi:10.1016/j.mtbio.2025.101854.
19. Maruf A, Wang Y, Luo L, Zhong Y, Nurhidayah D, Liu B, et al. Nanoerythrocyte membrane-enveloped ROS-responsive 5-aminolevulinic acid prodrug nanostructures with robust atheroprotection. Part Part Syst Charact. 2020;37(5):2000021. doi:10.1002/ppsc.202000021.
20. Mohammed F, Ke W, Mukerabigwi JF, Japir M, Ibrahim AAM, Wang A, et al. ROS-responsive polymeric nanocarriers with photoinduced exposure of cell-penetrating moieties for specific intracellular drug delivery. ACS Appl Mater Interfaces. 2019;11(35):31681–92. doi:10.1021/acsami.9b10950.
21. Oh H, Jeong E, Lee JS, Kim J, Lee D, Kim BS, et al. ROS-responsive PEGylated ferrocene polymer nanoparticles with improved stability for tumor-selective chemotherapy and imaging. Mater Today Bio. 2023;22:100774. doi:10.1016/j.mtbio.2023.100774.
22. Wang Y, Zheng J, Lin J, Ye K, Wei P. Mitochondria-targeting and ROS-responsive nanocarriers via amphiphilic TPP-PEG-TK-Ce6 for nanoenabled photodynamic therapy. Adv Polym Technol. 2022;2022(1):1178039. doi:10.1155/2022/1178039.
23. Wang D, Jiang Q, Shen R, Peng L, Zhou W, Meng T, et al. ROS-responsive nanoparticles targeting inflamed colon for synergistic therapy of inflammatory bowel disease via barrier repair and anti-inflammation. Nano Res. 2024;17(6):5409–23. doi:10.1007/s12274-024-6435-6.
24. Wang Y, Ming Y, Yu Z, Xu Z, Zou M, Chen C, et al. ROS-responsive cationic polymers with intrinsic anti-inflammatory activity for intracellular protein delivery. Biomacromolecules. 2025;26(4):2268–81. doi:10.1021/acs.biomac.4c01593.
25. Sun CY, Cao Z, Zhang XJ, Sun R, Yu CS, Yang X. Cascade-amplifying synergistic effects of chemo-photodynamic therapy using ROS-responsive polymeric nanocarriers. Theranostics. 2018;8(11):2939–53. doi:10.7150/thno.24015.
26. Xiong Q, Zhang H, Fang Y, Feng H, Cheng J, Li Z, et al. ROS-responsive and-regulated polysaccharide-based nanodelivery system enabling phloem-targeted fungicide delivery for apple vascular disease control. Adv Funct Mater. 2026;36(11):e11596. doi:10.1002/adfm.202511596.
27. Yang B, Wang K, Zhang D, Sun B, Ji B, Wei L, et al. Light-activatable dual-source ROS-responsive prodrug nanoplatform for synergistic chemo-photodynamic therapy. Biomater Sci. 2018;6(11):2965–75. doi:10.1039/c8bm00899j.
28. Zhang Z, Lu Z, Yuan Q, Zhang C, Tang Y. ROS-Responsive and active targeted drug delivery based on conjugated polymer nanoparticles for synergistic chemo-/photodynamic therapy. J Mater Chem B. 2021;9(9):2240–8. doi:10.1039/d0tb02996c.

29. Zhong XC, Shi MH, Liu HN, Chen JJ, Wang TT, Lin MT, et al. Mitochondrial targeted doxorubicin derivatives delivered by ROS-responsive nanocarriers to breast tumor for overcoming of multidrug resistance. Pharm Dev Technol. 2021;26(1):21–9. doi:10.1080/10837450.2020.1832116.
30. Zhang Y, Li Y, Huang S, Zhang H, Lin Q, Gong T, et al. Enhanced anti-metastatic therapy with down-regulation of heparinase expression by ROS-responsive micellar nanoparticles. Nanoscale. 2021;13(36):15267–77. doi:10.1039/d1nr02964a.
31. Zhou Z, Han J, Lang P, Zhang M, Shu H, Zhang L, et al. ROS-responsive self-assembly nanoplatform overcomes hypoxia for enhanced photodynamic therapy. Biomater Sci. 2024;12(19):5105–14. doi:10.1039/d4bm00712c.
32. Yang M, He F, Cai C, Wang Y, Shao J, Zhang W, et al. Nerve growth factor/angiogenin gene activated dermal bioscaffold for nerve repair in cutaneous wound healing. Nano Res. 2025;18(3):94907193. doi:10.26599/nr.2025.94907193.
33. Zhang B, Xue R, Sun C. Rational design of ROS-responsive nanocarriers for targeted X-ray-induced photodynamic therapy and cascaded chemotherapy of intracranial glioblastoma. Nanoscale. 2022;14(13):5054–67. doi:10.1039/d2nr00436d.
34. Zhang J, Zhang J, Zhang S, Yang W, Yang W, Guo J, et al. Dual-barrier traversing liposomes with ROS-responsive rigidity tuning for oral ischemic stroke therapy. J Control Release. 2025;385(13):113955. doi:10.1016/j.jconrel.2025.113955.
35. Yao Y, Wang L, Ding J, Pan X, Yang L, Guo C, et al. Nerve growth factor loaded hypotonic eye drops for corneal nerve repair. J Control Release. 2025;380(4):71–84. doi:10.1016/j.jconrel.2025.01.080.

Received: 05 November 2025; Accepted: 12 February 2026; Published: XX xxx 2026